Nanoscale Research Letters
a SpringerOpen Journal

NANO EXPRESS Open Access

Controlled fabrication of Sn/TiO_2 nanorods for photoelectrochemical water splitting

Bo Sun[1], Tielin Shi[1], Zhengchun Peng[2], Wenjun Sheng[1], Ting Jiang[1] and Guanglan Liao[1*]

Abstract

In this work, we investigate the controlled fabrication of Sn-doped TiO_2 nanorods (Sn/TiO_2 NRs) for photoelectrochemical water splitting. Sn is incorporated into the rutile TiO_2 nanorods with Sn/Ti molar ratios ranging from 0% to 3% by a simple solvothermal synthesis method. The obtained Sn/TiO_2 NRs are single crystalline with a rutile structure. The concentration of Sn in the final nanorods can be well controlled by adjusting the molar ratio of the precursors. Photoelectrochemical experiments are conducted to explore the photocatalytic activity of Sn/TiO_2 NRs with different doping levels. Under the illumination of solar simulator with the light intensity of 100 mW/cm^2, our measurements reveal that the photocurrent increases with increasing doping level and reaches the maximum value of 1.01 mA/cm^2 at −0.4 V versus Ag/AgCl, which corresponds to up to about 50% enhancement compared with the pristine TiO_2 NRs. The Mott-Schottky plots indicate that incorporation of Sn into TiO_2 nanorod can significantly increase the charge carrier density, leading to enhanced conductivity of the nanorod. Furthermore, we demonstrate that Sn/TiO_2 NRs can be a promising candidate for photoanode in photoelectrochemical water splitting because of their excellent chemical stability.

Keywords: TiO_2 nanorods; Sn doping; Photoelectrochemical water splitting

Background

Growing global energy demand and increasing concern for climate change have aroused the interest in new technologies to harness energy from renewable sources while decreasing dependence on fossil fuels [1,2]. One of the most attractive approaches is to produce hydrogen by solar water splitting, because of the high energy density of hydrogen and zero harmful byproduct after combustion as a fuel [3,4]. Since the first report of the photoelectrochemical water splitting using n-type TiO_2 in 1972 [5], TiO_2 has drawn more and more attentions in this field and is regarded as one of the most promising materials as photoanode for solar water splitting, considering its high chemical stability, low cost, and nontoxicity [6,7].

Early efforts in using TiO_2 material for solar water splitting were mainly focused on the nanoparticle-based thin films for their large surface area-to-volume ratios. However, the high charge carrier recombination and low electron mobility at the grain boundary limit the performance of the films [8,9]. Recently, researches shifted to the one-dimensional nanostructure including nanorods [10-12], nanotubes [13-15], and nanowires [16,17]. Various fabrication processes were developed for the synthesis of TiO_2 nanorods, nanowires, or nanotubes, such as catalyst-assisted vapor–liquid-solid (VLS) [16], hydrothermal process [10], electrochemical anodization [18,19], etc. However, TiO_2 is a wide band gap semiconductor, only absorbing UV-light, which suppresses its further applications. Considerable efforts have been devoted to improve the photon absorption and photocatalytic activity of TiO_2 nanostructures, including synthesizing branched structures [20], exposing its active surface [21], hydrogen annealing process [22,23], and sensitizing with other small band gap semiconductor materials such as PbS [14], CdSe [24], and CuInS [25].

Doping with other elements to tune the band gap of TiO_2 is another efficient method to improve the photocatalytic activity. N, Ta, Nb, W, and C have been successfully incorporated into TiO_2 photoanode and been demonstrated with enhanced photoconversion efficiency [26-29]. Besides, the SnO_2/TiO_2 composite fibers have also emerged and showed well photocatalytic property

* Correspondence: guanglan.liao@hust.edu.cn
[1]State Key Laboratory of Digital Manufacturing Equipment and Technology, Huazhong University of Science and Technology, Wuhan 430074, China
Full list of author information is available at the end of the article

[30,31]. Based on these researches, we expect that the incorporation of Sn into TiO_2 would be an attractive approach since the small lattice mismatch between TiO_2 and SnO_2 is beneficial for the structural compatibility and stability. Meanwhile, the doping would significantly increase the density of charge carriers and lead to a substantial enhancement of photocatalytic activity. In this work, we successfully realized the controlled incorporation of Sn into TiO_2 nanorods by a simple solvothermal synthesis method and investigated the role of Sn doping for enhanced photocatalytic activity in photoelectrochemical water splitting.

Methods

In our experiments, a transparent conductive fluorine-doped tin oxide (FTO) glass was ultrasonically cleaned in acetone and ethanol for 10 min, respectively, and then rinsed with deionized (DI) water. Twenty-five milliliters DI water was mixed with 25 mL concentrated hydrochloric acid (37%) in a Teflon-lined stainless steel autoclave. The mixture was stirred for several minutes before adding of 0.8 mL tetrabutyl titanate (TBOT). Then, 0–80 μL of Tin tetrachloride ($SnCl_4$) solution was added for the synthesis of Sn-doped TiO_2 nanorods (Sn/TiO_2 NRs), followed by another several minutes stirring. Subsequently, the clean FTO substrate was placed into the Teflon-liner. The synthesis process was conducted in an electric oven, and the reaction temperature and time were 180°C and 6 h, respectively, for most of the experiments. After that, the autoclave was cooled, and the FTO substrate was taken out and rinsed with DI water. Finally, the sample was annealed at 450°C in quartz tube furnace (Thermo Scientific, Waltham, MA, USA) for 2 h in the air to remove the organic reactant and enhance the crystallization of the nanorods. For the synthesis of pristine TiO_2 nanorods, the process was all the same, except for the elimination of the Sn precursor. The white nanorods film was detached from the FTO substrate with a blade and then added into ethanol followed by sonication for about 20 min. After that, two drops of the ultrasonically dispersed solution were dropped onto the copper grid and dried by heating in the ambient air for examination. To distinguish the samples with different doping levels, the Sn/TiO_2 NRs were marked in the form of Sn/TiO_2-a%, where a% is the molar ratio of $SnCl_4$/TBOT.

The morphology and lattice structure of the nanorods were examined by the field-emission scanning electron microscopy (FESEM, JSM-7600 F, JEOL, Akishimashi, Tokyo, Japan) and field-emission transmission electron microscopy (FTEM, Tecnai G2 F30, FEI, Hillsboro, OR, USA). The energy-dispersive X-ray spectroscopy (EDX) combined with FSEM and FTEM was employed to detect the element composition of Sn/TiO_2 NRs. To further determine the crystal structure and possible phase changes after introducing Sn doping, the crystal structure was examined with X-ray diffraction (XRD, PW3040/60, PANalytical, Almelo, The Netherlands). Moreover, X-ray photoelectron spectroscopy (XPS, VG Multilab 2000 X, Thermo Electron Corp., Waltham, MA, USA) was employed to determine the chemical composition and states of the nanorods. The binding energy of the C 1 s (284.6 eV) was used for the energy calibration, as estimated for an ordinary surface contamination of samples handled under ambient conditions.

To measure the performance of photoelectrochemical (PEC) water splitting, the exposed FTO was covered with a layer of silver paste and connected to Cu wires with solder. The silver paste, solder, edge and some part of the film were sealed with polydimethylsiloxane (PDMS) or epoxy, in which only a well-defined area about 1 cm^2 of the white film was exposed to the electrolyte. A glass vessel filled with 400 mL 1 M KOH was used as the PEC cell, and a class AAA solar simulator (Oriel 94043A, Newport Corporation, Irvine, CA, USA) with the light intensity of 100 mW/cm^2 was used as light source. The photocurrent and electrochemical impedance spectra were collected by electrochemical station (AUTOLAB PGSTAT302N, Metrohm Autolab, Utrecht, The Netherlands). Line sweep voltammograms were obtained at the scan rate of 20 mV/S. A Pt slice acting as the counter electrode and a standard Ag/AgCl reference electrode (containing saturated KCl solution) were used for the PEC measurements. The water splitting process in PEC cell was schematically illustrated in (Additional file 1: Figure S1).

Results and discussion

The morphology of the Sn/TiO_2 nanorods synthesized under different conditions was depicted in Figure 1. Here, Figure 1a,d shows the top view and side view of the nanorods that were synthesized at 150°C for 18 h, Figure 1b,e shows the nanorods synthesized at 180°C for 6 h, and Figure 1c,f shows the nanorods synthesized at 180°C for 4 h, respectively. It reveals that the diameters of the nanorods are about 200, 100, and 80 nm, accordingly, each nanorod consisting of a bundle of thinner nanorods with rectangular top facets. The side view confirms that all the nanorods were grown almost perpendicularly to the FTO substrates, and the average length of the nanorods is 2.1, 2.1, and 1.5 μm, respectively. In order to optimize the surface area-to-volume ratio for PEC water splitting, and enhance the comparability between the nanorods with and without Sn doping, the reaction conditions for median Sn/TiO_2 nanorods density (Figure 1b,e) were selected for all the remaining experiments in this paper. A wide range of precursor molar ratios ($SnCl_4$/TBOT = 0% to 3%) in the initial

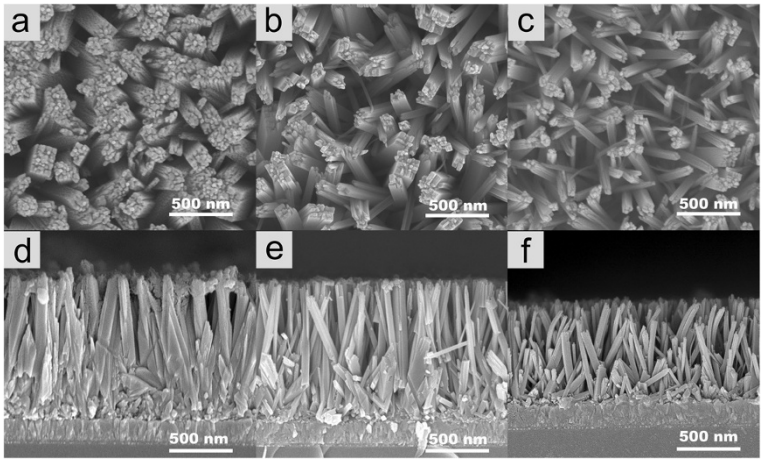

Figure 1 SEM images of the nanorods synthesized under different conditions. (a) and **(d)** at 150°C for 18 h; **(b)** and **(e)** at 180°C for 6 h; **(c)** and **(f)** at 180°C for 4 h.

reactant mixture were used for Sn doping, and almost no noticeable morphology change was observed, except that when the molar ratio reached to 8% the difference turned out to be obvious, as shown in (Additional file 1: Figure S2).

Figure 2 displays the TEM images and SAED pattern of a typical Sn/TiO_2 NR. Although the nanorods detached from the FTO substrate have cracked as shown in the inset of Figure 2a, we can clearly find out that the diameter is about 100 nm, consistent with that measured by SEM in Figure 1b. The image of the nanorod tip confirms that each individual nanorod indeed consists of a bundle of thinner nanorods, with the diameters about 10 to 20 nm. The high-resolution transmission electron microscopy (HRTEM) image collected from the edge of the nanorods reveals that the typical Sn/TiO_2 NR has a single crystalline structure with the interplanar spacings of 0.32 nm and 0.29 nm, in accordance with the d-spacings of (110) and (001) planes of rutile TiO_2, respectively. These results indicate that the Sn/TiO_2 NR grows along the <001> direction. The sharp SAED pattern as shown in the inset of Figure 2b further confirms that the Sn/TiO_2 NR is a single crystalline rutile structure.

Figure 3 illustrates the element composition of a representative Sn/TiO_2-0.5% NR obtained by EDX. Figure 3a shows the high-angle annular dark-field (HAADF) scanning TEM image of the nanorod, while Figure 3b,c,d are elemental mappings of Ti, O, and Sn, respectively, collected from the nanorod within the rectangular region marked in Figure 3a. Although this percentage of Sn/Ti has approached to the detection limit of EDX and some background noise have kicked in, we can find that Sn atoms have been incorporated over the entire TiO_2 nanorod obviously in Figure 3d. Besides, the Sn/Ti ratios of all the detected samples are close to the $SnCl_4$/TBOT molar ratios as shown in (Additional file 1: Figure S3).

To further determine the crystal structure and possible phase changes after Sn doping, we collected the XRD spectra from pristine TiO_2 NRs and Sn/TiO_2 NRs

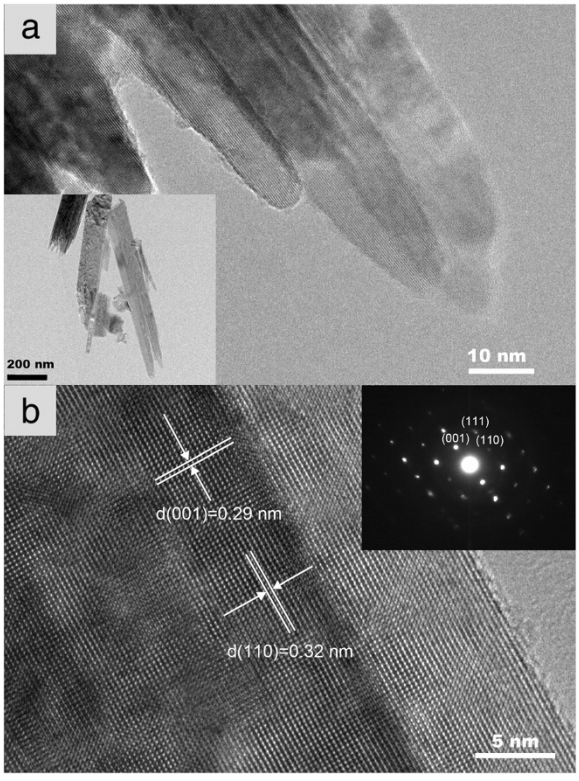

Figure 2 TEM images and SAED pattern. (a) TEM image of the tip of a typical Sn/TiO_2 NR shown in the inset, **(b)** HRTEM image of edge of the nanorod, where the inset is SAED pattern of the nanorod.

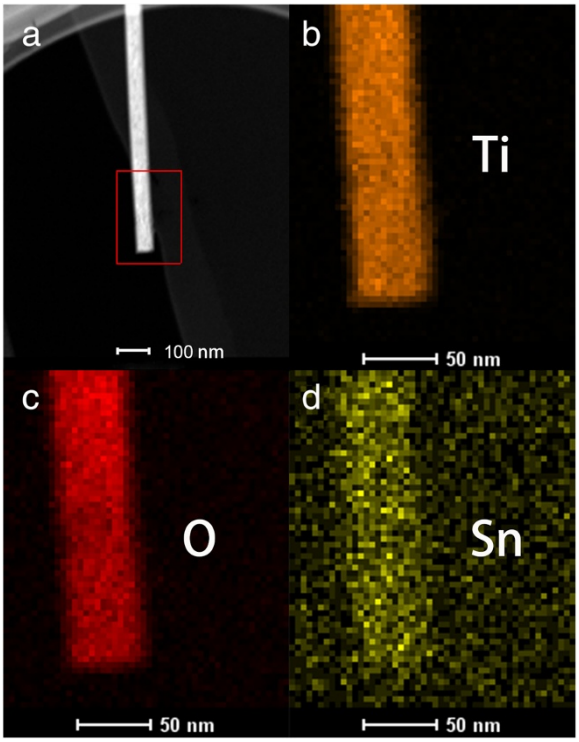

Figure 3 HAADF scanning TEM image and elemental mappings of a Sn/TiO_2-0.5% NR. (a) HAADF scanning TEM image, **(b), (c),** and **(d)** is the elemental mappings of Ti, O, and Sn, collected from the nanorod within the rectangular region marked in **(a)**.

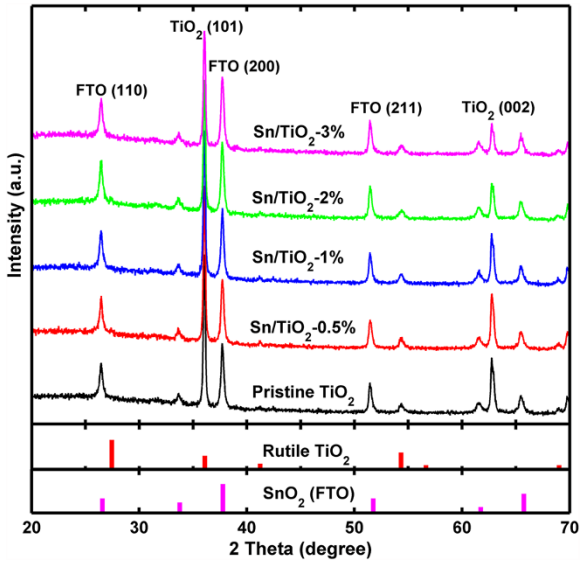

Figure 4 XRD patterns of pristine TiO_2 NRs and Sn/TiO_2 NRs synthesized with different precursor molar ratio. The reference spectra (JCPDS No. 21–1276 and No. 46–1088) were plotted for comparison.

synthesized with different precursor molar ratio, as shown in Figure 4, in which the typical diffraction peaks of the patterns have been marked. It confirms that the Sn/TiO_2 NRs have a tetragonal rutile TiO_2 crystal structure (JCPDS No. 21–1276), which is the same as the pristine TiO_2 NRs. Even for the highly doped sample (Sn/TiO_2-3%), there is no obvious change in diffraction peaks. We infer that the Sn atoms just replace Ti atoms in some spots without destroy the rutile TiO_2 crystal structure as schematically illustrated in (Additional file 1: Figure S4). Noteworthy is that the relative intensity of (002) peaks seems to decrease as the doping level exceed 2%. This change may result from the fact that the perpendicularity of the nanorods to the substrate has reduced, as demonstrated in (Additional file 1: Figure S2).

To investigate the changes of the surface composition and chemical states of TiO_2 NRs after introducing Sn doping, the XPS spectra collected from the pristine TiO_2 NRs and two representative Sn/TiO_2 NRs samples with initial $SnCl_4$/TBOT molar ratio of 1% and 3% are compared in Figure 5a. The XPS peaks of the TiO_2 NRs (with or without Sn doping) at about 458.1 and 463.9 eV correspond to Ti $2p_{3/2}$ and Ti $2p_{1/2}$ (Figure 5b), and the XPS peak at about 529.4 eV corresponds to O 1 s state (Figure 5c), respectively. In Figure 5d, the two peaks of the spectra collected from Sn/TiO_2-3% NRs at about 486.2 and 494.8 eV correspond to Sn $3d_{5/2}$ and Sn $3d_{3/2}$, which confirms that the main dopant is Sn^{4+}. Compared to the pristine TiO_2 NRs, the Ti and O peaks of Sn/TiO_2 NRs show a small positive shift (as shown in Figure 5b,c), which suggests a certain electron drain from the Ti^{4+} in the oxide matrix due to the presence of Sn^{4+}, considering their difference in electronegativity (Sn = 1.96 vs. Ti = 1.54) [32]. This further confirms that the Sn dopant is indeed mixed into TiO_2 NRs at the atomic level, agreeing well with the XRD results as shown in Figure 4. Besides, quantitative analysis of the spectra reveals that the Sn/Ti molar ratio is about 1.2% for Sn/TiO_2-1% NRs and 3.2% for Sn/TiO_2-3% NRs, respectively.

Next, the photocatalytic activities of the Sn/TiO_2 NRs with different Sn doping levels for PEC water splitting are discussed. Figure 6a displays the line sweep voltammograms measured from pristine TiO_2 NRs (black), Sn/TiO_2-0.5% NRs (red), and Sn/TiO_2-1% NRs (green), and the current of the pristine TiO_2 NRs in dark is plotted in black dotted line for comparison. The photocurrent density of pristine TiO_2 is 0.71 and 0.77 mA/cm^2 at the potential of −0.4 and 0 V versus Ag/AgCl, while the value increases to 0.85 and 0.93 mA/cm^2 for the Sn/TiO_2-0.5% NRs and reaches 1.01 and 1.08 mA/cm^2 for the Sn/TiO_2-1% NRs. To further explore the effect of Sn doping on the photocatalytic activity, the photocurrent measurements were conducted for a series of samples synthesized with the precursor molar ratio from 0% to 3%. The photocurrent density ratios between Sn/TiO_2 NRs

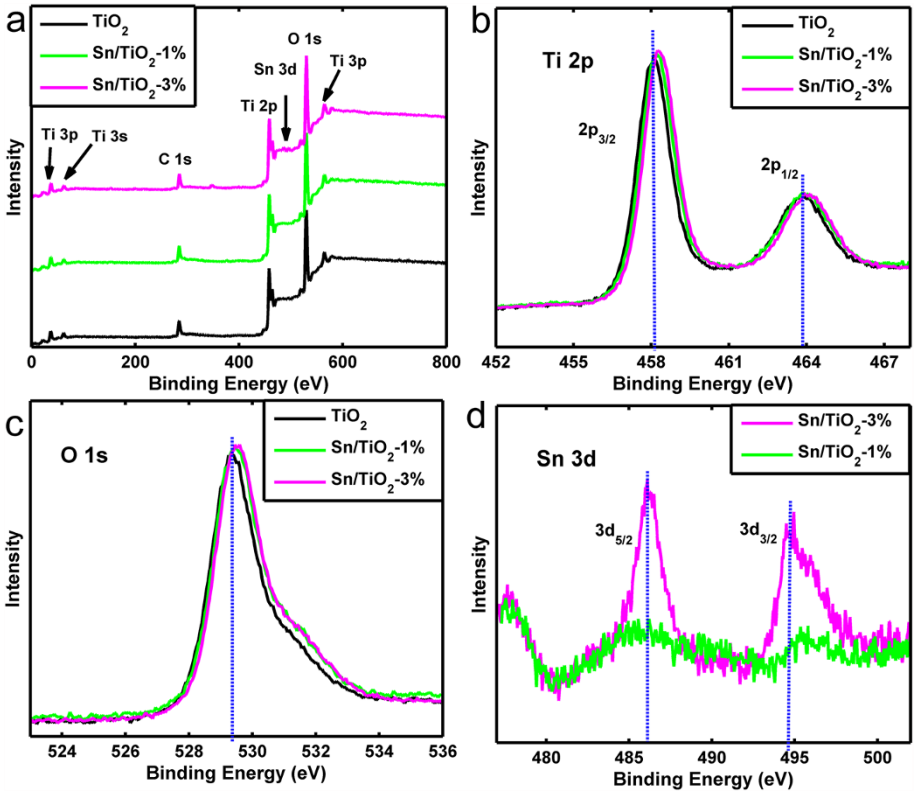

Figure 5 XPS survey spectra. (a) Low-resolution XPS survey spectra of the pristine TiO_2 NRs and Sn/TiO_2 NRs with different Sn doping, **(b)** Ti 2p XPS spectra, **(c)** O 1 s XPS spectra; **(d)** Sn 3d XPS spectra.

and pristine TiO_2 NRs photoanodes measured at −0.4 V versus Ag/AgCl are depicted in Figure 6b, where the inset is the optical image of the packaged Sn/TiO_2 NR photoanodes. The results reveal that the photocurrent first increases as the doping level rises and reaches the max value of 142 ± 10% at precursor molar ratio of 1%, which corresponds to up to about 50% enhancement compared to pristine TiO_2 NRs sample, and then decreases gradually and drops to a value even lower than that of a pristine nanorods.

To analyze the efficiency of Sn/TiO_2 NRs for PEC water splitting quantitatively, the photoconversion efficiency is calculated as follow [33]:

$$\eta = J(1.23 - V)/P,$$

where J is the photocurrent density at the measured potential, V is the applied voltage versus reversible hydrogen electrode (RHE), and P is the power intensity of 100 mW/cm^2 (AM 1.5G). The RHE potential can be converted from the Ag/AgCl reference electrode [23]

$$\text{Voltage (RHE)} = \text{Voltage (Ag/AgCl)} + 1.0\text{V}.$$

As shown in Figure 6c, the pristine TiO_2 NRs achieve the efficiency of 0.48%, while the Sn/TiO_2-0.5% NRs and Sn/TiO_2-1% NRs achieve the efficiencies of 0.59% and 0.69% at about −0.53 V versus Ag/AgCl, about 23% and 44% enhancement, respectively. The photocatalytic properties of TiO_2 and Sn/TiO_2-1% nanorods with different morphology were depicted in (Additional file 1: Figure S5), which further supports our choice of the reaction conditions for median nanorods density. These results suggest that appropriate incorporation of Sn atoms can significantly enhance the photocatalytic activity of TiO_2 NRs and lead to substantial increase of the photocurrent density and photoconversion efficiency.

The time-dependent measurements also have been carried out on the three samples, as shown in Figure 6d. With repeated on/off cycles of illumination from the solar simulator, the three samples display highly stable photocurrent densities of 0.71, 0.86 and 1.01 mA/cm^2 at −0.4 V versus Ag/AgCl, respectively. These measurements have been repeated in several months, and there is no noticeable change happened. This indicates that the Sn/TiO_2 NRs possess highly chemical and structural stability for PEC water splitting, which is another critical factor to evaluate their potentials as the photoanode material.

To investigate the role of Sn doping on the enhanced photocatalytic activity, especially for its influence on the electronic properties of TiO_2 NRs, we have conducted

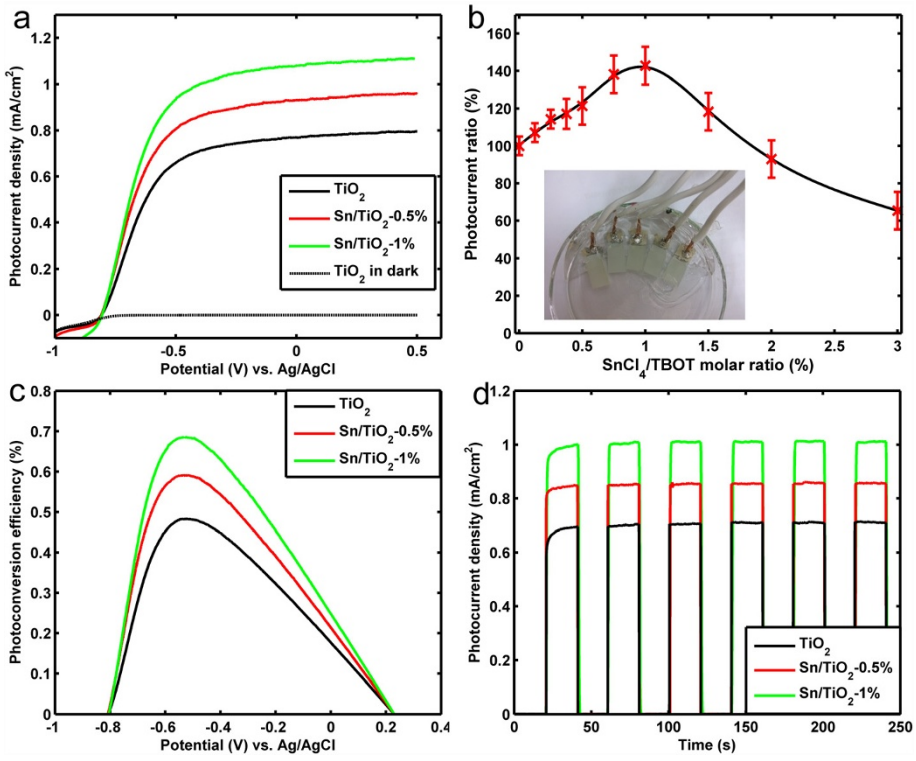

Figure 6 Photocatalytic properties of the nanorods. (a) Line sweep voltammograms measured from pristine TiO_2 NRs (black), Sn/TiO_2-0.5% NRs (red), and Sn/TiO_2-1% NRs (green). The current of the pristine TiO_2 NRs in dark is plotted for comparison. **(b)** Photocurrent density ratios between Sn/TiO_2 NRs and pristine TiO_2 NRs photoanodes measured at −0.4 V versus Ag/AgCl, and the inset is optical photo of a few typical packaged samples. **(c)** Photoconversion efficiency of the three samples as a function of applied voltage versus Ag/AgCl. **(d)** Time-dependent photocurrent density of the three samples at repeated on/off cycles of illumination from the solar simulator.

electrochemical impedance measurement on the pristine TiO_2 and Sn/TiO_2 NRs with different doping levels at the frequency of 5 kHz in dark as shown in Figure 7. All the samples measured show a positive slope in the Mott-Schottky plots, as expected for TiO_2 which is a well-known n-type semiconductor. Importantly, the Sn-doped TiO_2 NRs samples show substantially smaller slopes than that of the pristine TiO_2 NRs, suggesting a significantly increase of charge carrier densities. Furthermore, the slope decreased gradually as the precursor molar ratio increased from 0.5% to 3%, which confirms the role of Sn doping on increasing the charge carrier density. The carrier densities of these nanorods can be calculated from the slopes of Mott-Schottky plots using the equation [23]

$$N_d = \left(\frac{2}{e_0 \varepsilon \varepsilon_0}\right)\left[\frac{d\left(\frac{1}{C^2}\right)}{dV}\right]^{-1},$$

where N_d is the charge carrier density, e_0 is the electron charge, ε is the dielectric constant of TiO_2 ($\varepsilon = 170$) [23], and ε_0 is the permittivity of vacuum. The calculated charge carrier densities of the pristine TiO_2, Sn/TiO_2-1%

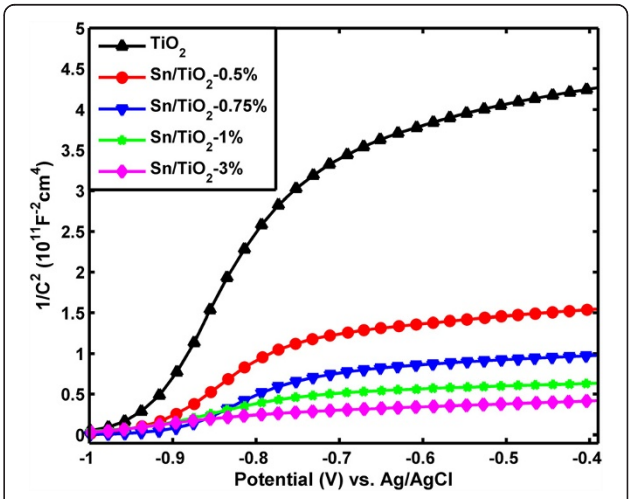

Figure 7 Mott-Schottky plots for the pristine TiO_2 NRs and Sn/TiO_2 NRs with different doping levels. The data were collected at a frequency of 5 kHz in the dark.

and Sn/TiO_2-3% NRs are 5.5×10^{17}, 7.85×10^{18}, and 1.25×10^{19} carries/cm^3, respectively. We note that the Mott-Schottky method is derived based on a flat electrode model and may have errors in determining the accurate value of charge carrier density of the Sn/TiO_2 NRs, since we use the planar area instead of the effective surface area for calculation [34]. Nevertheless, the qualitative comparison of the carrier density of these samples is valid, given that there is almost no difference between the morphology of pristine TiO_2 and Sn/TiO_2 NRs.

As oxygen vacancy serving as electron donor has been accepted generally as the main cause for the n-type conductivity of TiO_2 [35], we expect that the incorporation of Sn atoms may lead to the increase of oxygen vacancy which is responsible for the enhanced photocatalytic activity. Besides, other reported effects may also be at work. For instance, the formation of mixed-cation composition ($Sn_xTi_{1-x}O_2$) at the interface and associated modulation of electronic properties may facilitate the exciton generation and separation [30]. The potential difference of TiO_2 and SnO_2 may promote the photoelectron migration from TiO_2 to SnO_2 conducting band with decreasing combination, allowing both of the photogenerated electrons and holes to participate in the overall photocatalytic reaction [31]. However, the photocurrent of Sn/TiO_2-3% NRs is lower to the pristine TiO_2. This may be rationalized as the overly high Sn doping level upshifting the TiO_2 band gap and creating much more interfaces, which substantially reduces the light absorption efficiency and impedes the photogenerated charge separation.

Conclusions

In summary, we have successfully realized the controlled incorporation of Sn into TiO_2 NRs to enhance the photocatalytic activity for PEC water splitting. Sn concentration is well controlled by adjusting the precursor molar ratio. We studied the crystal structure of the obtained Sn/TiO_2 NRs, which is the same as the pristine TiO_2 NRs. The PEC measurements reveal that the photocurrent reaches the maximum value of 1.01 mA/cm^2 at –0.4 V versus Ag/AgCl with a Sn/Ti molar ratio of about 1%, which corresponds to up to about 50% enhancement compared to the pristine TiO_2 NRs. The Mott-Schottky plots indicate that the incorporation of Sn into TiO_2 NRs can significantly increase the charge carrier density, hence improving the conductivity of TiO_2 NRs and leading to the increase of photocurrent. Besides, the Sn/TiO_2 NRs exhibit excellent chemical stability which further promotes them to be a promising candidate for photoanode in photoelectrochemical water splitting devices. With the enhanced conductivity, we believe the Sn/TiO_2 NRs can also serves as substitution for pure TiO_2 structures in other optoelectronic applications including photocatalysis, photodetectors, solar cells, etc.

Additional file

Additional file 1: Figure S1. Schematic illustration of the water splitting process in PEC cell. **Figure S2.** SEM images of the Sn/TiO_2 NRs with different doping levels, (a) Sn/TiO_2-0.5% NRs, (b) Sn/TiO_2-8% NRs. **Figure S3.** EDX spectra measured from a series of Sn/TiO_2 NRs, with initial $SnCl_4$/TBOT ratio range from 0.5% to 8%, (a) 0.5%, (b) 1%, (c) 1.5%, (d) 2%, (e) 3%, (f) 8%, the marked values in the spectra are detected Sn/Ti ratio. **Figure S4.** A supercell for modeling the crystal structure of the Sn/TiO_2 NRs. **Figure S5.** The photocatalytic properties of TiO_2 and Sn/TiO_2 nanorods with different morphology, (a) photoconversion density, (b) photoconversion efficiency.

Competing interests

The authors declare that they have no competing interests.

Authors' contributions

BS carried out experimental work, analyzed the data, and prepared the manuscript. TLS participated in the studies and supervised the research work. ZCP improved the manuscript. WJS and TJ participated in the experimental work. GLL participated in the studies, improved the manuscript, and supervised the research work. All authors read and approved the final manuscript.

Acknowledgements

The authors are grateful for the financial supports by the National Natural Science Foundation of China (grant nos. 51175210 and 51222508).

Author details

[1]State Key Laboratory of Digital Manufacturing Equipment and Technology, Huazhong University of Science and Technology, Wuhan 430074, China. [2]Technology Manufacturing Group, Intel Corporation, 2501 NW 229th Ave, Hillsboro, OR 97124, USA.

Received: 2 September 2013 Accepted: 27 October 2013
Published: 5 November 2013

References

1. Chen YW, Prange JD, Dühnen S, Park Y, Gunji M, Chidsey CED, McIntyre PC: **Atomic layer-deposited tunnel oxide stabilizes silicon photoanodes for water oxidation.** *Nat Mater* 2011, **10:**539–544.
2. Davis SJ, Caldeira K, Matthews HD: **Future CO_2 emissions and climate change from existing energy infrastructure.** *Science* 2010, **329:**1330–1333.
3. Murdoch M, Waterhouse GIN, Nadeem MA, Metson JB, Keane MA, Howe RF, Llorca J, Idriss H: **The effect of gold loading and particle size on photocatalytic hydrogen production from ethanol over Au-TiO_2 nanoparticles.** *Nat Chem* 2011, **3:**489–492.
4. Bai HW, Liu ZY, Sun DD: **The design of a hierarchical photocatalyst inspired by natural forest and its usage on hydrogen generation.** *Int J Hydrogen Energy* 2012, **37:**13998–14008.
5. Fujishima A, Honda K: **Electrochemical photolysis of water at a semiconductor electrode.** *Nature* 1972, **238:**37–38.
6. Roy P, Berger S, Schmuki P: **TiO_2 nanotubes synthesis and applications.** *Angew Chem Int Ed* 2011, **50:**2904–2939.
7. Szymanski P, El-Sayed MA: **Some recent developments in photoelectrochemical water splitting using nanostructured TiO_2: a short review.** *Theor Chem Acc* 2012, **131:**1202.
8. Hendry E, Koeberg M, O'Regan B, Bonn M: **Local field effects on electron transport in nanostructured TiO_2 revealed by terahertz spectroscopy.** *Nano Lett* 2006, **6:**755–759.
9. Fravventura MC, Deligiannis D, Schins JM, Siebbeles LDA, Savenije TJ: **What limits photoconductance in anatase TiO_2 nanostructures? A real and imaginary microwave conductance study.** *J Phys Chem C* 2013, **117:**8032–8040.
10. Liu B, Aydil ES: **Growth of oriented single-crystalline rutile TiO_2 nanorods on transparent conducting substrates for dye-sensitized solar cells.** *J Am Chem Soc* 2009, **131:**3985–3990.
11. Feng XJ, Shankar K, Varghese OK, Paulose M, Latempa TJ, Grimes CA: **Vertically aligned single crystal TiO_2 nanowire arrays grown directly on**

transparent conducting oxide coated glass: synthesis details and applications. *Nano Lett* 2008, **8**:3781–3786.
12. Oh JK, Lee JK, Kim HS, Han SB, Park KW: **TiO_2 branched nanostructure electrodes synthesized by seeding method for dye-sensitized solar cells.** *Chem Mater* 2010, **22**:1114–1118.
13. Zhang ZH, Hossain MF, Takahashi T: **Photoelectrochemical water splitting on highly smooth and ordered TiO_2 nanotube arrays for hydrogen generation.** *Int J Hydrogen Energy* 2010, **35**:8528–8535.
14. Ratanatawanate C, Xiong CR, Balkus KJ Jr: **Fabrication of PbS quantum dot doped TiO_2 nanotubes.** *ACS Nano* 2008, **2**:682–1688.
15. Hou Y, Li XY, Zhao QD, Quana X, Chen GH: **TiO_2 nanotube/Ag–AgBr three-component nanojunction for efficient photoconversion.** *J Mater Chem* 2011, **21**:18067–18076.
16. Park YS, Lee JS: **Morphology control of single crystalline rutile TiO_2 nanowires.** *Bull Korean Chem Soc* 2011, **32**:3571–3574.
17. Chen JZ, Ko WY, Yen YC, Chen PH, Lin KJ: **Hydrothermally processed TiO_2 nanowire electrodes with antireflective and electrochromic properties.** *ACS Nano* 2012, **6**:6633–6639.
18. Albu SP, Ghicov A, Macak JM, Schmuki P: **250 μm long anodic TiO_2 nanotubes with hexagonal self-ordering.** *Phys Status Solidi (RRL)* 2007, **1**:R65–R67.
19. Paramasivam I, Macak JM, Selvam T, Schmuki P: **Electrochemical synthesis of self-organized TiO_2 nanotubular structures using anionic liquid ($BMIM\text{-}BF_4$).** *Electrochim Acta* 2008, **54**:643–648.
20. Cho IS, Chen ZB, Forman AJ, Kim DR, Rao PM, Jaramillo TF, Zheng XL: **Branched TiO_2 nanorods for photoelectrochemical hydrogen production.** *Nano Lett* 2011, **11**:4978–4984.
21. Liu XL, Zhang HM, Yao XD, An TC, Liu PR, Wang Y, Peng F, Carroll AR, Zhao HJ: **Visible light active pure rutile TiO2 photoanodes with 100% exposed pyramid-shaped (111) surfaces.** *Nano Res* 2012, **5**:762.
22. Chen X, Liu L, Yu PY, Mao SS: **Increasing solar absorption for photocatalysis with black hydrogenated titanium dioxide nanocrystals.** *Science* 2011, **331**:746–750.
23. Wang GM, Wang HY, Ling YC, Tang YC, Yang XY, Fitzmorris RC, Wang CC, Zhang JZ, Li Y: **Hydrogen-treated TiO_2 nanowire arrays for photoelectrochemical water splitting.** *Nano Lett* 2011, **11**:3026–3033.
24. Bang JH, Kamat PV: **Solar cells by design: photoelectrochemistry of TiO_2 nanorod arrays decorated with CdSe.** *Adv Funct Mater* 2010, **20**:1970–1976.
25. Zhou ZJ, Yuan SJ, Fan JQ, Hou ZL, Zhou WH, Du ZL, Wu SX: **CuInS2 quantum dot-sensitized TiO_2 nanorod array photoelectrodes: synthesis and performance optimization.** *Nanoscale Res Lett* 2012, **7**:652.
26. Hoang S, Guo SW, Hahn NT, Bard AJ, Mullins CB: **Visible light driven photoelectrochemical water oxidation on nitrogen-modified TiO_2 nanowires.** *Nano Lett* 2012, **12**:26–32.
27. Hoang S, Guo S, Buddie MC: **Coincorporation of N and Ta into TiO_2 nanowires for visible light driven photoelectrochemical water oxidation.** *J Phys Chem C* 2012, **116**:23283–23290.
28. Das C, Roy P, Yang M, Jha H, Schmuki P: **Nb doped TiO_2 nanotubes for enhanced photoelectrochemical water-splitting.** *Nanoscale* 2011, **3**:3094–3096.
29. Cho IS, Lee CH, Feng Y, Logar M, Rao PM, Cai L, Kim DR, Sinclair R, Zheng XL: **Codoping titanium dioxide nanowires with tungsten and carbon for enhanced photoelectrochemical performance.** *Nat Comm* 2013, **4**:1723.
30. Pan J, M Hühne S, Shen H, Xiao LS, Born P, Mader W, Mathur SJ: **SnO_2-TiO_2 Core-shell nanowire structures: investigations on solid state reactivity and photocatalytic behavior.** *Phys Chem C* 2011, **115**:17265–17269.
31. Liu Z, Sun DD, Guo P, Leckie JO: **An efficient bicomponent TiO_2/SnO_2 nanofiber photocatalyst fabricated by electrospinning with a side-by-side dual spinneret method.** *Nano Lett* 2007, **7**:1081–1085.
32. Li J, Zeng HC: **Hollowing Sn-doped TiO_2 nanospheres via Ostwald ripening.** *J Am Chem Soc* 2007, **129**:15839–15847.
33. Walter MG, Warren EL, McKone JR, Boettcher SW, Mi Q, Santori A, Lewis NS: **Solar water splitting cells.** *Chem Rev* 2010, **110**:6446–6473.
34. Lin YJ, Zhou S, Sheehan SW, Wang DW: **Nanonet-based hematite heteronanostructures for efficient solar water splitting.** *J Am Chem Soc* 2011, **133**:2398–2401.
35. Janotti A, Varley JB, Rinke P, Umezawa N, Kresse G, Van de Walle CG: **Hybrid functional studies of the oxygen vacancy in TiO_2.** *Phys Rev B* 2010, **81**:085212.

doi:10.1186/1556-276X-8-462
Cite this article as: Sun *et al.*: Controlled fabrication of Sn/TiO_2 nanorods for photoelectrochemical water splitting. *Nanoscale Research Letters* 2013 **8**:462.